A Wearable, Multimodal Sensing System to Monitor Knee Joint Health

Caitlin N. Teague, *Student Member, IEEE*, J. Alex Heller, *Member, IEEE*, Brandi N. Nevius, Andrew M. Carek, Samer Mabrouk, Florencia Garcia-Vicente, Omer T. Inan, *Senior Member, IEEE*, and Mozziyar Etemadi, *Member, IEEE*

Abstract*—*Objective: **We designed and validated a wearable, multimodal sensor brace for knee joint health assessment.** ***Methods:*** **An embedded-, two-microcontroller-based approach is used to sample high-throughput, multi-microphone joint acoustics (46.875 kHz) as well as lower-rate electrical bioimpedance (EBI) (1/46.17 s), inertial (100 – 250 Hz), and skin temperature (1 Hz) data, and these data are saved onto microSD cards. Additionally, a flexible, 3D-printed brace houses the custom circuit boards and sensors to enable wearable sensing.** ***Results:*** **The system achieves 9 hours of continuous joint sound recording, while the EBI, inertial, and temperature sensors can sample for 35 hours using 500 mAh batteries. Further, for the entirety of these continuous recordings, there were no dropped samples for any of the sensors. Lastly, proof-of-concept measurements were used to show the system's efficacy for recording joint sounds and swelling data.** ***Conclusion:*** **This is, to the best of our knowledge, the first, completely untethered wearable system for multimodal knee health monitoring.** ***Significance:*** **The proposed smart brace may facilitate in-clinic or at-home measurements for joint health assessment.**

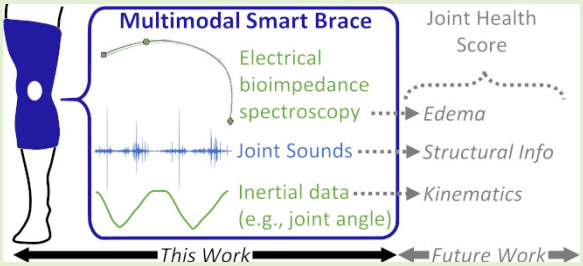

***Index Terms*—Embedded software, joint physiology, mHealth, rapid prototyping, wearable sensors.**

I. Introduction

WEARABLE technologies for healthcare represent a popular research area, as they can provide quantitative metrics during rehabilitation, enable long-term, at-home monitoring of chronic conditions, and facilitate preventative—versus reactive—medical interventions. Moreover, their low cost makes them accessible to broad subject populations and enables more frequent measures of biomarkers. Such technologies are particularly useful for areas of medicine where the diagnostic or evaluation tools are expensive, not readily available, or time-consuming.

Orthopedics—in particular joint health assessment—is an area where wearable devices may provide clinicians and patients with more readily available quantitative data. Recently, wearable sensing modalities for the knee joint have been explored to assess joint health. Such sensing modalities include the measurement of joint acoustics, edema, and activity via miniature microphones, electrical bioimpedance (EBI) circuitry, and inertial measurement units (IMUs), respectively. For example, joint acoustical emissions ("joint sounds") have been used to discriminate healthy subjects and those with osteoarthritis [1], [2], classify varying conditions of the patellofemoral joint [3], monitor improvements in kids with juvenile idiopathic arthritis after receiving effective medication [4], track rehabilitation improvements in athletes following an acute injury [5], and show changes in loading stresses on the joint [6]. Similarly, EBI has been used to detect swelling (edema) of the joint [7], and studies have demonstrated its efficacy for detecting changes in edema during injury recovery [8]. Lastly, researchers have leveraged IMUs to provide information about knee valgus/joint stability [9], range of motion [10], [11], and joint kinematics [12] on

Manuscript received April 10, 2020; accepted April 28, 2020. Date of publication May 14, 2020; date of current version August 14, 2020. This work was supported by the Defense Advanced Research Projects Agency (DARPA) Biological Technologies Office (BTO) ElectRx program through the Naval Information Warfare Center (NIWC) under Cooperative Agreement N66001-19-2-4002. The associate editor coordinating the review of this article and approving it for publication was Dr. Wan-Young Chung. *(Corresponding author: Caitlin N. Teague.)*

Caitlin N. Teague and Samer Mabrouk are with the School of Electrical and Computer Engineering, Georgia Institute of Technology, Atlanta, GA 30308 USA (e-mail: caitlin.n.teague@gmail.com).

J. Alex Heller, Andrew M. Carek, Florencia Garcia-Vicente, and Mozziyar Etemadi are with the Department of Biomedical Engineering, McCormick School of Engineering, Northwestern University, Evanston, IL 60208 USA, and also with the Department of Anesthesiology, Feinberg School of Medicine, Northwestern University, Evanston, IL 60208 USA (e-mail: mozzi@northwestern.edu).

Brandi N. Nevius is with the School of Mechanical Engineering, Georgia Institute of Technology, Atlanta, GA 30308 USA.

Omer T. Inan is with the School of Electrical and Computer Engineering, Georgia Institute of Technology, Atlanta, GA 30308 USA, and also with the Wallace H. Coulter Department of Biomedical Engineering, Georgia Institute of Technology, Atlanta, GA 30308 USA (e-mail: inan@gatech.edu).

Digital Object Identifier 10.1109/JSEN.2020.2994552

their own, while also providing contextual information when combined with other sensing modalities, such as noting the angular location at which joint sounds occur [13]. Ultimately, joint acoustics, edema, and kinematics aim to capture some underlying physiological state or anatomical change within the joint itself.

While these measures have shown promise for assessing the health of the knee, nearly all the work using these sensors has been conducted in-lab/in-clinic using benchtop data acquisition units, which are not conducive for realistic implementation of such systems. An embedded systems-based approach presents an attractive next step, as embedded systems can be used for rapid prototyping and deployment in early phases of research due to their availability, low cost, and extended battery life. With respect to IMUs and EBI systems for wearable applications, embedded-based approaches have been achieved [14]–[18], likely made readily feasible by operating at conveniently low sampling rates ($\leq$ 2 kHz). However, acquiring joint sounds, which have been captured in even the ultrasonic bandwidth [1] and may use multiple microphones arrayed around the knee [6], [13], pose greater sampling loads for embedded systems. Further, given the still-exploratory nature of joint health research, joint sounds cannot yet be compressed (e.g., to minimize data storage or transmission requirements) using lossy methods without compromising the potential feature space, though recent work by Athavale *et al.* suggests an encoding scheme of these signals is possible [19], and compression ratios of lossless methods need to be balanced with energy consumption, memory accesses, and overall hardware constraints, such as the available RAM [20]. For biomedical research, there has been minimal work that acquires audio in wearable-type settings; studies have often relied on the use of commercially available audio recorders or smart phones [21], [22], which cannot be readily integrated into a custom system, particularly one designed to be wearable. Conversely, custom embedded systems have been deployed in other fields such as environmental monitoring and underwater acoustics, though these systems have leveraged larger batteries, higher power consumption, and greater footprint overall [23]–[26] and/or are commonly limited to single-channel audio [27], [28]. As such, new techniques for recording data from multiple high- and low-bandwidth sensors must be explored to achieve wearable technologies.

In this work, we present a multimodal "smart" knee brace for joint health assessment, capturing joint sounds, EBI, inertial measures, and skin temperature. This is the first-ever wearable system, to the best of our knowledge, that combines monitoring of both knee physiology (i.e., swelling and kinematics) and structure (i.e., acoustics). In contrast to our group's prior work [13], [29], which involved benchtop hardware tethered to a laptop for data collection, this paper presents the hardware and firmware implementation of two fully embedded sub-systems and validation of their function. Importantly, we consider the robust sampling and saving of data, ensuring that no data packets are dropped. These embedded hardware systems were packaged in a flexible, 3D-printed "brace," providing an initial mechanical prototype for a wearable system. Lastly, we present proof-of-concept recordings of joint health data from a healthy subject, demonstrating the feasibility of the brace to be used for in-clinic or at-home studies. Ultimately, we envision the use of this smart brace to measure joint health data, which can then be processed with feature extraction and machine learning algorithms to provide a comprehensive and quantitative joint health score, equipping clinicians and patients with actionable data that may be used during rehabilitation following an acute injury or when titrating medication for disease management (Fig. 1).

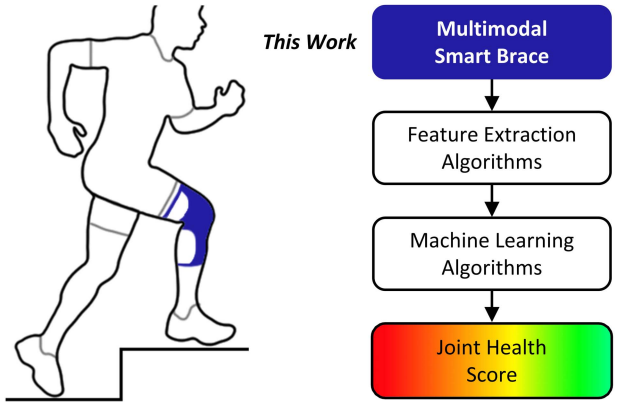

Fig. 1. Overview of the wearable, multimodal sensor brace for knee joint health assessment. Using this smart brace, sensor data can be extracted and used to provide physiologically significant information such as swelling, activity level, and joint angle. Ultimately, machine learning algorithms can be employed to provide a joint health score for use in various applications, including during rehabilitation after an acute injury and management of joint diseases, such as arthritis.

II. Embedded System Design

The system is comprised of two subsystems, currently located on two separate printed circuit boards (PCBs). The first system's purpose is to sample high-throughput audio data triggered by a switch, while the second system continuously samples lower-rate data from multiple sensors, specifically EBI, inertial, and temperature data. In this paper, these two boards are referred to as the audio and main board, respectively. A summary of the system and sensors is provided in Fig. 2.

This two-microcontroller design was used to ensure that packets are not dropped. Given the high data rate required by the microphones, a dedicated microcontroller is required to obtain data from an analog-to-digital converter (ADC) and write it to a microSD card as quickly as possible. Even with this sole purpose, the microcontroller fails to strictly meet SD card timing specifications, which is described in Section II-A-(3). Adding additional clock cycles to sample other sensors would further exacerbate this issue. Consequently, another microcontroller needed to sample from all other sensors. These subsystems were placed on separate boards so that the main board can be independently used for EBI measurement.

Importantly, these two boards are synchronized to provide important contextual information for joint sounds. For example, for joint sounds, IMUs provide joint angle, speed of the exercise, and exercise type, while for EBI, IMUs

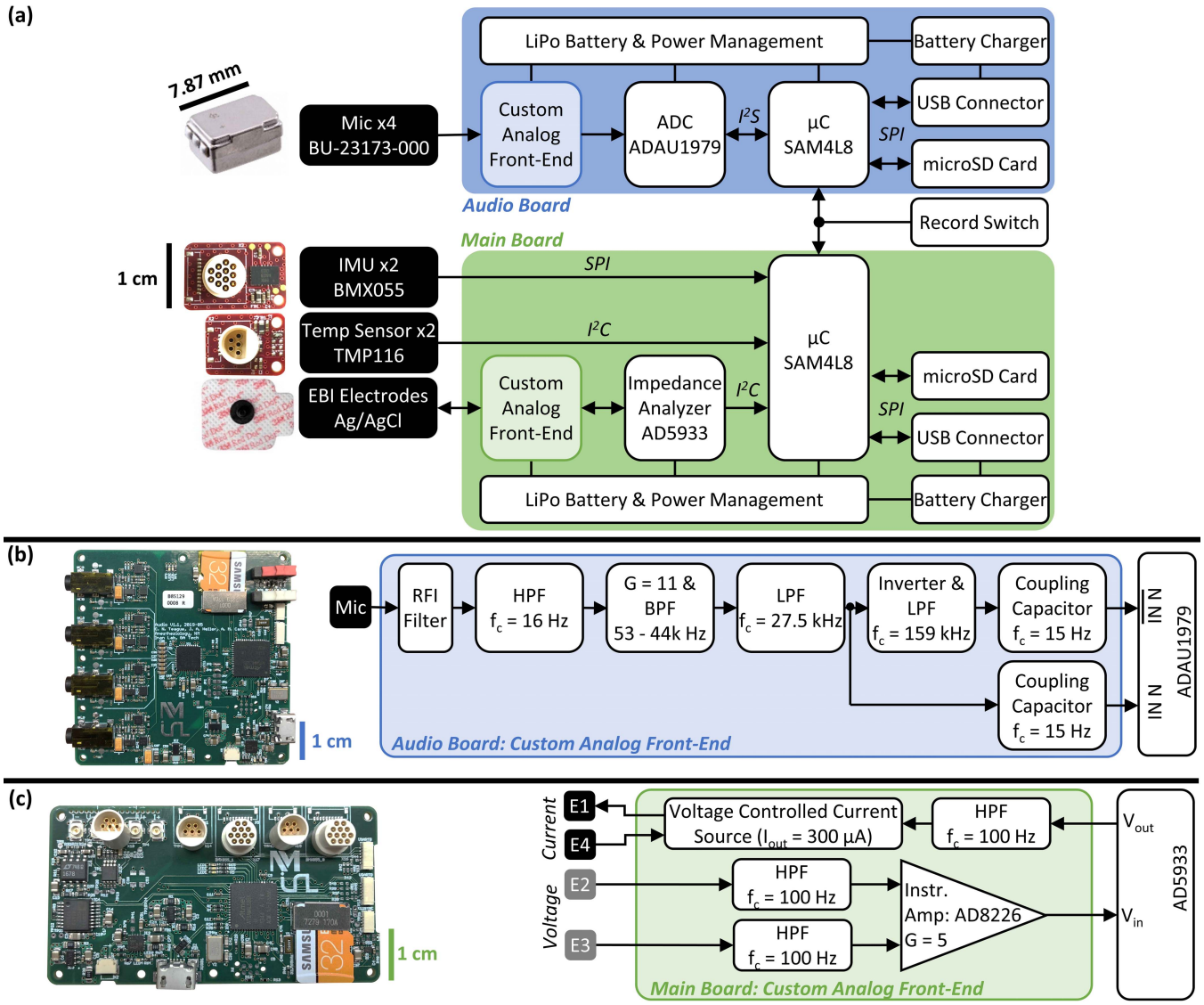

Fig. 2. Smart brace system and block diagram. (a) Overall system block diagram, which consists of two circuit boards synchronized via an interrupt pin controlled by a slide switch, "Record Switch." The main board consists of a microcontroller (μC), which continuously samples data from (1) two inertial measurement units with three-axis accelerometer and gyroscope data, (2) two temperature sensors, and (3) electrical bioimpedance sensing hardware connected to the body via four Ag/AgCl gel electrodes. The sampled data are saved onto a microSD card. These data can later be read by a computer via USB, interfaced by an on-board microUSB connector. The audio board consists of a custom analog front-end, which applies gain and filters to four contact microphones. These four microphones are sampled by an ADC that transfers data to the microcontroller to save onto a microSD card. Both circuits have their own batteries, battery chargers, and power management systems to provide digital and analog power to different components. (b) Photo of the audio printed circuit board and block diagram of the custom analog front-end for conditioning the microphone signals. (c) Photo of the main circuit board and block diagram (reproduced from [33]) of the electrical bioimpedance circuit.

determine the orientation of the limb and can be used to gate processing of data compromised by motion artifacts. Similarly, the temperature sensors provide skin temperature, which can be used for interpreting changes in signals (e.g., edema) that are a result of environmental changes and are not due to underlying physiological changes. Accordingly, the system is aware of the context surrounding the physiological and structural health measurements, which should improve the robustness and relevance of the data obtained for assessing knee health.

Both boards use a SAM4L8 (Microchip Technology Inc., Chandler, AZ) microcontroller. It was selected for its low power modes, extensive digital communication modules, and inclusion of floating-point arithmetic, which future designs could leverage for on-board processing. Furthermore, the SAM4L is a 32-bit microcontroller, which is an important feature for efficiently reading audio data and minimizing counter roll-over of the 32.768 kHz crystal, which was clocked down to 4096 Hz. When it is used to record sample times, absolute timing of samples can be synchronized between the boards simply with an interrupt pin because overflow occurs at a time (12 days) that exceeds the battery life.

A. Audio Printed Circuit Board Design

A photo and block diagram of the audio PCB are shown in Fig. 2(a) and (b). This system consists of four contact

microphones, a custom analog front-end, a four-channel analog-to-digital converter (ADC), a microcontroller (MCU), and a microSD card.

1) Microphones and Audio Analog Front-End: The system permits four microphone channels. We selected miniature contact microphones (BU-23173-000, Knowles Electronics LLC., USA) for their low noise, small size, and wide bandwidth. Moreover, our previous work has shown their efficacy for evaluation of mechanical stress on the knee [6]. A contact microphone is essentially a wide bandwidth accelerometer that detects the vibrations of the skin in response to underlying acoustic emissions from the joint.

Each single-ended microphone signal was passed through a custom analog front-end (AFE). A block diagram of the AFE is shown in Fig. 2(b). Following a radio frequency interference filter and a passive high pass filter ($f_c = 16$ Hz), the signal was amplified (gain of 11) and filtered (53 Hz – 44 kHz) using an audio operational amplifier (op-amp) (LTC6240, Analog Devices, Inc., Norwood, MA), which was selected for its high gain bandwidth product and low noise. Given the prevalence of the use of 100 Hz as a sample rate for IMU-based knee joint kinematics in the literature, a high-pass filter cutoff of 53 Hz (i.e., ~50 Hz) was selected to reduce motion artifacts from saturating the amplifier. The signal was then low-pass filtered at 27.6 kHz via a second-order Sallen-Key to reduce aliasing during sampling. Though higher-order filters are generally preferred to provide sharp roll-off to prevent aliasing, the design leveraged the sigma-delta architecture of the ADC; sigma-delta ADCs oversample the inputs at a much higher rate than the sampling frequency, increasing the Nyquist frequency and allowing for a more gradual roll-off analog filters. Limiting the anti-aliasing filter to one op-amp and four passive components helped minimize power consumption and PCB footprint. The next stage consisted of an inverter—with low pass filtering ($f_c = 159$ kHz)—to create a differential signal. For this stage, highly matched passive components were employed to minimize error between the inverting and non-inverting inputs. Operating in differential mode allowed for a higher effective number of bits given these components do not add more noise than bits gained, and this was experimentally verified. Finally, the differential signals were AC coupled; this capacitor combined with a resistor internal to the ADC to form a final high pass filter ($f_c = 15$ Hz). The AFE regulator's shutdown pin allowed this circuitry to be dynamically turned on and off by the MCU.

2) Analog-to-Digital Conversion and Data Transfer: The differential signals were sampled by a standalone ADC. We selected the ADAU1979 (Analog Devices, Norwood, MA) for its for its high bit depth (16 or 24 bits), low noise (-95 dB total harmonic distortion), and four-channel, simultaneous-sampling capability. Our prior studies were completed using 16-bit data acquisition systems—with both higher possible input voltage ranges and single-ended configurations—and demonstrated differences between different populations of subjects (healthy vs. injured) as well as different mechanical loading conditions within a given subject [5], [6], suggesting the 16-bit configuration should suffice for extracting physiologically relevant features using this new hardware.

The SAM4L8 only has one inter-IC sound (I^2S) channel and operates using a standard two-channel, stereo mode (i.e., a left and right channel on a single data bus). I^2S consists of three communication lines: (1) SDATA, which gives the serial sound data; (2) BCLK, which provides timing for each individual bit of SDATA; and (3) LRCLK, which specifies the left or right channel of SDATA. This conflicts with the default configuration of the ADC, which splits the four audio channels onto two different data busses when using I^2S. To transfer all four channels on one data bus, the time-division multiplexing (TDM) communication protocol—with respect to the ADC—must be used. TDM is an extended I^2S protocol allowing for multiple channels (slots) to be fit within one left/right channel, allowing for all four signals to be transmitted over a single SDATA bus. We use TDM4 to fit two signals within one channel. Using the 16-bit ADC data width, two signals may fit within one 32-bit LRCLK window. Accordingly, the MCU is programmed to expect 32-bit LRCLK channels, and the ADC fills each left/right channel with two slots of 16-bit data. Post-processing later splits the data into distinct microphone signals.

3) Saving Data to a microSD Card: For saving the audio data stream, we employ the MCU's direct memory access (DMA). The DMA allows the I^2S module to directly save data to memory without processing intervention. The data are saved using a circular buffer with the DMA working with one half of the buffer at a time. We leverage the MCU's reload buffer feature (i.e., a pointer to the next location to write data when the buffer is full), which helps prevent dropping packets since the DMA always has an address at which to write data. Once half a buffer is full, the MCU records the time as read from a 32.768 kHz crystal (clocked at 4096 Hz). It then saves the data to the microSD card. We write 22 016 bytes (43 512-byte sectors) every 58.7 ms. The SD card specification indicates a maximum write time of 250 ms [30]. However, because the data throughput is so high and RAM limited, we do not meet this constraint. Because we record the time when a buffer is full, we can determine in post-processing if samples are dropped due to slow SD card writes or quality of the card.

A simple file system was implemented on the microSD card with FAT16 compatibility [31]. Each file is defined by its starting address on the microSD card and its length (i.e., an offset from this starting address). Each half buffer—a multiple of 512-byte blocks for write-efficiency—is written as raw binary data to the SD card to be interpreted by the PC.

B. Main Printed Circuit Board Design

A photo and block diagram of the main PCB is shown in Fig. 2(a) and (c). This system continuously samples from the EBI system, IMUs, and temperature sensors.

1) Main Board Sensors: The BMX055 (Bosch Sensortec GmbH, Kusterdingen, Germany) is a three-axis accelerometer, gyroscope, and magnetometer. Though the magnetometer is not used in this work, future iterations of the system may choose to sample from this sensor to provide complete orientation estimates [32]. This sensor was chosen for its low-noise sensors and digital output interface, SPI. Though the current consumption is higher than other IMUs currently available, we selected it for this first iteration as an initial proof-of-concept.

To measure temperature, we selected the TMP116 (Texas Instruments Inc., Dallas, TX) for its high bit-depth and accuracy, on-board averaging, low current consumption, digital output (I^2C), and ability to trigger multi-sensor synchronized readings.

The EBI system is based off our group's previous work [33]. For this work, we use the AFE and calibration scheme developed by Mabrouk *et al.* on this new board [33]; note that the firmware—particularly how EBI is sampled with respect to other sensors as well as the audio board—is specific to this work. Briefly, the EBI system consists of an impedance analyzer integrated circuit (IC) (AD5933, Analog Devices, Inc., Norwood, MA) connected to a custom AFE to interface the body. Typically, the AD5933 provides an excitation voltage and receives a current measurement as part of a two-electrode configuration. However, the two-electrode configuration includes the electrode-skin impedance as part of the measurement, lowering the dynamic range, accuracy, and resolution. Moreover, this configuration does not strictly limit current as required by safety specifications (IEC 60601-1-11) [34].

To mitigate these issues, a four-electrode configuration was used. The outer electrodes (E1 and E4 in Fig. 2(c)) source current through the tissue, while a high impedance instrumentation amplifier (IA) (AD8226, Analog Devices, Inc., Norwood, MA) connected by the inner electrodes (E2 and E3) measures the voltage, thus neglecting the skin-electrode impedance. The injected current is sourced via a voltage-controlled current source, delivering 280 μA_{rms} (0A DC) to the body, complying with safety requirements. A block diagram of the AFE is provided in Fig. 2(c). EBI measurements are performed in sweeps consisting of 256 equidistant-frequencies at 371 Hz ranging from 5 kHz – 99.605 kHz. For each frequency, a 16-bit real and imaginary impedance component is recorded.

2) Sampling Scheme for the Main Board: Data from the sensors are continuously sampled. The sampling scheme for this system is similar to that described in [31]; lower-power sensors—when new samples are ready—drive wake-up periods for the MCU, consuming less power since the MCU (1) is only active when sampling or saving data and (2) does not waste unnecessary cycles polling sensors to determine if data are ready. As such, the MCU is in a low-power mode for most of the time and only wakes up to an active state when it receives a data-ready interrupt.

C. Computer Data Extraction Software and Time Syncing

Data saved on the microSD cards must be extracted at some point for analysis. A custom program was developed in C# for transferring data from the microSD card to the computer directly, alleviating the need for a user or study coordinator to interact with the microSD cards or hardware directly. When the PCBs are connected to the computer via a microUSB cable, the device is recognized by the computer as a USB device. Opening the custom program lists connected devices and their respective files, cataloging each file size and creation date/time. A single mouse click automatically downloads all the files from the device, saving them to a folder on the computer. Lastly, the program transfers date/time information to the device. This time synchronization allows for precise timekeeping, simplifies synchronization of multiple devices, and permits timestamp-based file naming according to when a recording was started.

III. An Initial Brace Proof-of-Concept

A. Brace Design

To demonstrate the system's translation towards a feasible wearable device, the embedded system was integrated into a wearable "brace" as shown in Fig. 3. The brace is comprised of three major components: the circuit box and two sensor housings located proximal and distal to the patella.

The circuit box, 3D-printed using a polylactic acid (PLA) material, contains the main and audio PCBs, two batteries (LP-523334 3.7 V 500 mAh with PCM, Shenzhen PKCELL Battery Co., Ltd, Guangdong Sheng, China), and switches for initiating and stopping recordings. The circuit box itself is 7.5 × 7.7 × 3.9 cm. An exploded view of the circuit box assembly is shown in Fig. 3(c).

The sensor housings (Fig. 3(d)) serve as enclosures for the IMU and temperature sensors and include two electrode snaps for the EBI measurement (I and V electrodes) along with one additional snap that provides mounting support and is not electrically connected. The sensor housings are 3D-printed using a thermoplastic polyurethane material (NinjaFlex, NinjaTek, Manheim, PA). Its flexible nature serves multiple purposes; it allows the brace to easily conform to different leg shapes and sizes and to provide some mechanical compliance as the subject moves. For reference, all blue components shown in Fig. 3 are printed using this material. The electrode snaps are exposed on the subject-facing side to accommodate standard gel electrodes. Moreover, a slot in this inner surface exposes the temperature sensor, allowing for skin temperature measurements. The temperature sensor PCBs are coated with an aerosolized rubber (Plasti Dip, Plasti Dip International, Blaine, Minnesota) to protect the subject's skin from directly interfacing active and exposed circuit components while also providing the board protection from moisture, such as a subject's sweat.

The sensors and electrodes are connected to the circuit box via custom cables. Each cable—one to the IMU, temperature sensor, and both electrodes—are bundled into one larger cable assembly using silicone heat shrink. This method consolidates the four cables into one assembly while maintaining flexibility and permits sanitation.

B. Affixing the Brace

An important aspect of deploying a brace, particularly for at-home studies where ease-of-use for the subject is paramount, is consistent placement of sensing elements to (1) ensure the sensors acquire the desired data at specified anatomical locations and (2) facilitate valid longitudinal data comparisons. These considerations are essential for both joint sounds and EBI measurements; for joint acoustics, the positioning of the microphones with respect to the joint may influence the type of sounds measured, while EBI electrode spacing must be maintained to capture the same segment of the limb and thus the same gross tissue volume.

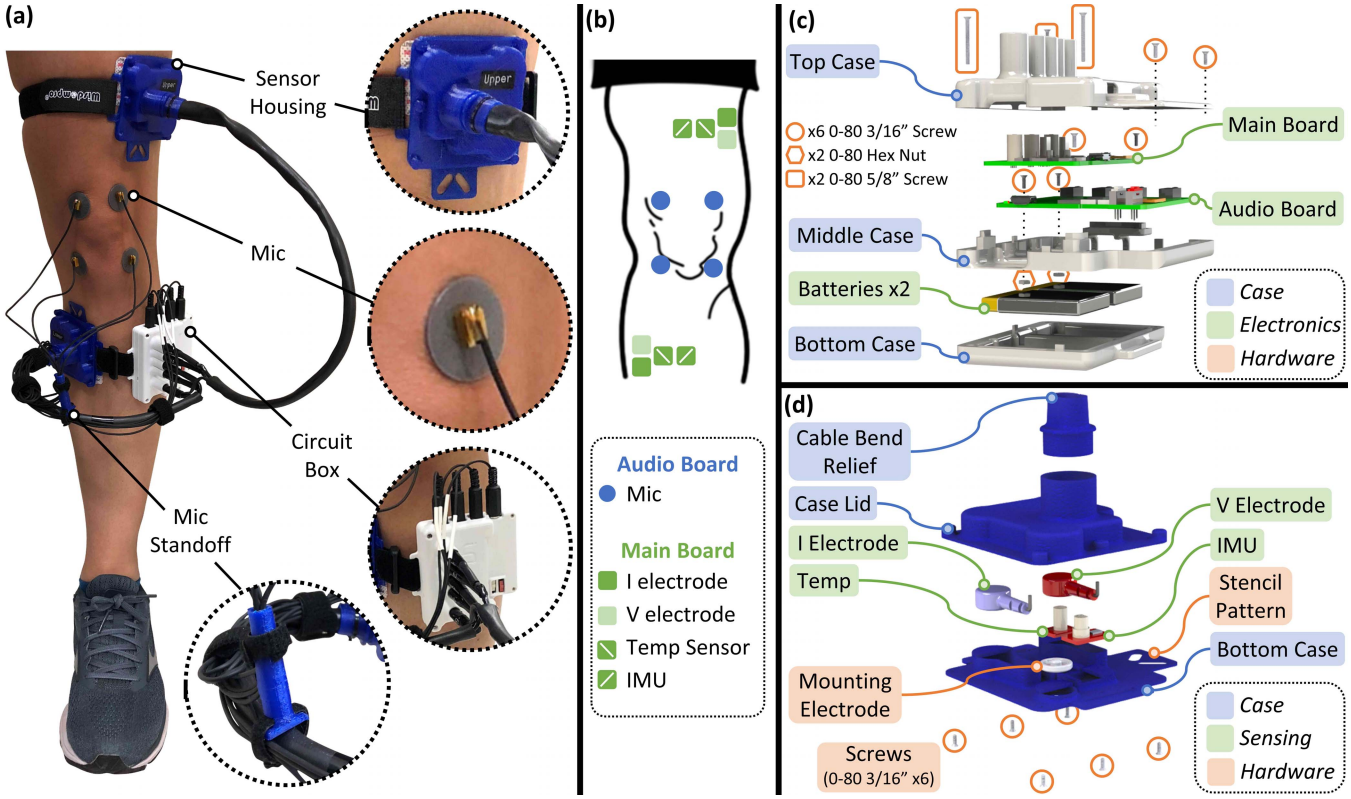

Fig. 3. Initial brace prototype. (a) The brace worn on a subject's left knee. There are three major system components: the circuit box and two sensor housing units. The sensor housings and circuit boxes are attached to the leg via Velcro straps, and the sensor housings are further adhered using two electrical bioimpedance (EBI) electrodes and a third, non-electrically connected electrode. Lastly, microphones are mounted both proximal and distal to the patella using double-sided tape stickers. A "microphone (mic) standoff" is used to route the microphone cables away from the leg to prevent noise caused by inadvertent pulling and/or tapping of the cables on the skin. (b) Approximate locations of the various sensors (for a left knee) as sampled by each board. (c) An exploded view of the assembled circuit box, which houses both PCBs and batteries. (d) An exploded view of one of the sensor housings, which contains two EBI electrodes (one for current (I) and one for voltage (V)), an electrode used for mounting (not electrically connected), an inertial measurement unit (IMU), and a temperature sensor.

To enable correct and consistent placement of the brace on any given subject, a "stencil" approach was developed as illustrated in Fig. 4. The stencil is a flexible, 3D-printed piece that provides areas to mark (with a marker) the subject's skin with the appropriate mounting locations. The stencil is configured with a curvature that fits against the distal or proximal edge of the patella, serving as an anatomical site for consistent sensor placement. Notably, multiple sized stencils—or even stencils with varying patella curvature—are required to accommodate subjects of different height and weight. The stencil contains slanted slots (angled at 45°) at a fixed distance from the patella for positioning the sensor housings. The sensor housings contain these same slots such that the housing can be aligned (Fig. 4(c)) and subsequently affixed to the skin, leveraging the EBI and mounting electrodes for adhesion and is further assisted by a Velcro strap. The angled nature of the slots constrains the placement of the sensor housing with respect to the sagittal and coronal planes, which are denoted as the x- and y- orientations in Fig. 4(a). Additionally, round holes in the stencil note microphone locations at the lateral and medial sides of the patella and quadriceps tendons when the stencil is positioned distally or proximally, respectively, and the microphones are then attached to the skin using double-sided adhesive pads (Lavalier Adhesive Stickies, Rycote, Rycote Microphone Windshields Ltd, Gloucestershire, United Kingdom).

However, correct placement of the microphones is not the only consideration; given they interface the audio board via long, free-hanging cables, the microphones can be susceptible to noise. These cables may introduce noise into the joint sound measurement by hitting other cables, tapping on the skin, and/or pulling on the microphone during articulation. To help prevent such instances, a "microphone standoff" (Fig. 3(a)) is used to route the cables away from the leg, provide sufficient slack throughout the entire range of motion, and consolidate the cables such that they do not touch parts of the brace and/or other cables. In this way, the microphone standoff emulates in-lab setups where cable management can be highly controlled.

C. Proof-of-Concept Recordings on Human Subjects

Institutional Review Board (IRB) approval was obtained from Northwestern University, the Georgia Institute of Technology, and the Navy's Human Research Protection Office (HRPO) to evaluate the device on human subjects. As a proof of concept, we measured signals from a single healthy subject (male, age: 33 years, height: 198 cm,

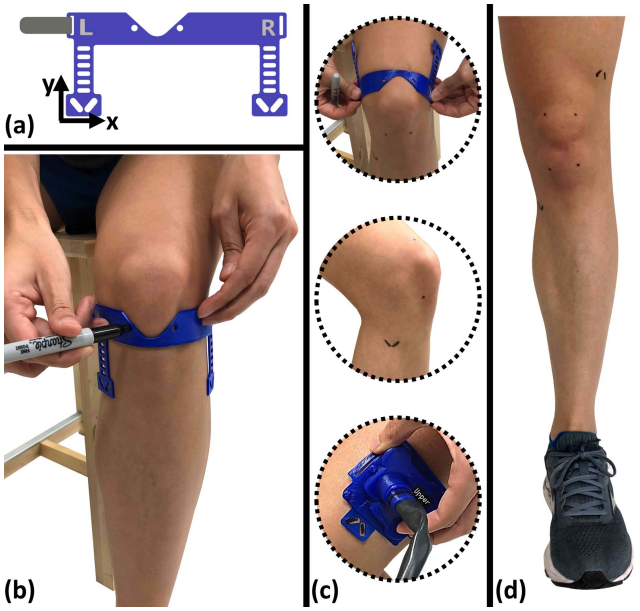

Fig. 4. The stencil mechanism for mounting the microphones and sensor housings. (a) A rendering of the stencil shape. The curvature is used to fit the proximal or distal edge of the patella, providing a consistent anatomical reference. The round holes are used for marking the microphone locations, while the angled slots are used for locating the position of the thigh strap. By angling the slots, both x- and y- orientation constraints are achieved. (b) Aligning the stencil to the distal edge of the patella. In this position, the distal microphone locations are marked (as shown) as well as the pattern for mounting the distal sensor housing. (c) Positioning the stencil proximally for the thigh markings (top), example of the stencil markings as shown from the medial side (middle), and aligning the proximal sensor housing with the angled-slot stencil marking (bottom). (d) The final stencil markings for the microphones and sensor housings.

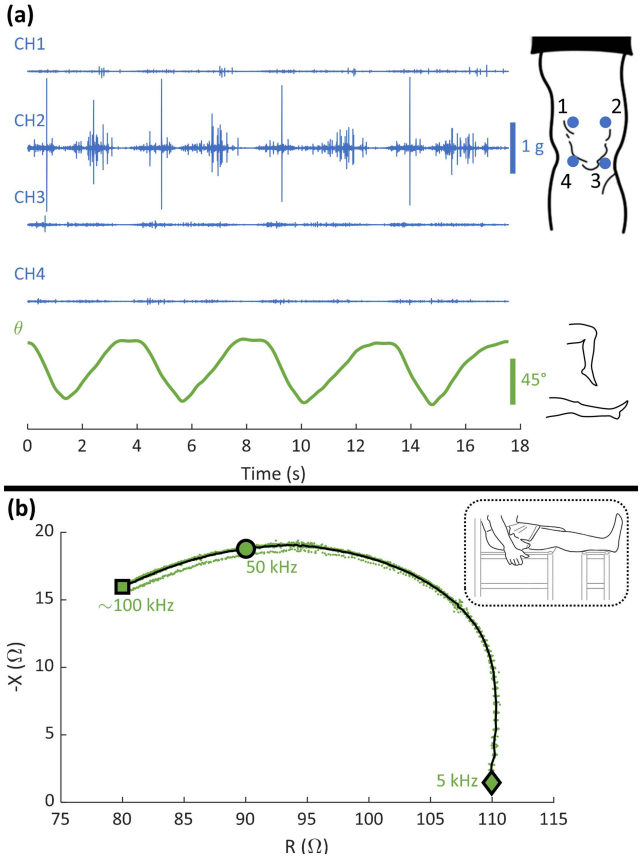

Fig. 5. Proof-of-concept recordings from a single subject. (a) Joint sounds (blue) recorded for four flexion/extension exercises using four microphones from the positions indicated. The flexion angle (green) is also provided. Importantly, significant acoustic emissions occur at similar joint angles for repeated exercises. (b) Electrical bioimpedance (EBI) sweep from 5 – 96.605 kHz plotted for 10 impedance sweeps (green) and are within 1 Ω of the overall ensemble average across the sweeps (black). Specific frequencies are marked for reference. The measurement was recorded with the subject positioned as shown in the inset. During this measurement, the average temperature recorded was 30.4° C.

weight: 79 kg) performing protocols established in previous studies [29]; specifically, for the joint sound measurement, the subject completed 10 cycles of unloaded, seated flexion/extension exercises, while the EBI measurement was conducted with the subject in a relaxed, seated position with his legs fully extended and supported (Fig. 5(b) inset) for 10 sweeps. Given that prior work has already considered the use of these signals as quantitative physiological markers of joint health across multiple populations [29], and as the focus of this work is to outline the hardware for sampling across multiple sensors in a wearable form factor, we chose to present the results from a single, representative subject as a means to benchmark the feasibility of collecting robust data in a typical use case.

For the purpose of this paper, processing was limited to enabling visualization of the signals of interest. Joint sounds from the four microphones were bandpass filtered (1 kHz – 10 kHz) and plotted against joint flexion angle, which was computed according to the algorithm presented by McGrath *et al.* [35]. The raw EBI data was converted to actual impedance values according to the calibration scheme by Mabrouk *et al.* [33]. Ensemble averaging—or sample-by-sample averaging across multiple datasets—was applied across the sweeps to provide a mean impedance sweep curve.

IV. Design and Proof-of-Concept Results and Discussion

A. System Characterization

Tables I and II provide a summary of the audio and main board technical specifications, respectively. Note the current consumptions reported were measured using an Agilent Digital Multimeter (34410A, Keysight Technologies, Santa Rosa, CA) in series with each board's battery and streamed to a computer (via an Agilent 82357B USB/GPIB Interface High-Speed USB 2.0 cable, Keysight Technologies, Santa Rosa, CA).

For the audio board, a minimum 7-hour battery life is achieved with a 500 mAh battery. When waiting to record, the analog circuitry and ADC are powered down, while the MCU is in a low-power mode, averaging a ~330 μA wait current. When recording, the average current (with floating inputs) is ~45.9 mA with average peak currents when writing to the microSD card at ~70 mA. Lastly, the measured frequency response through the ADC is 62.17 Hz – 22.84 kHz with a low-pass roll-off of approximately –1117 dB/decade,

TABLE I
AUDIO BOARD SYSTEM SPECIFICATIONS

Parameter	Value
Power Consumption – Data Collection [a, b]	~45.9 mA
Power Consumption – Sleep	~330 µA
Sample Rate	46.875 kHz
Size	5.5 cm x 5.5 cm
Battery Life (using 500 mAh battery) [b]	> 7 h
Frequency Range [c]	62.17 Hz – 22.84 kHz
Gain	20.75 dB
Minimum detectable signal	786 µg
Data Storage Capacity	Card dependent

[a] Recorded with floating inputs
[b] Dependent on SD card, number of recordings, and microphone inputs
[c] Measured response

TABLE II
MAIN BOARD SYSTEM SPECIFICATIONS

Parameter	Value
Power Consumption – Average [a, b]	~14.3 mA
Battery Life (using 500 mAh battery) [a, b]	> 33 h
Size	3.5 cm x 6.5 cm
Electrical Bioimpedance	
Sample Rate	1 sweep/46.17 s (21.7 mHz)
Frequency Range	5 kHz – 99.605 kHz
Frequency Resolution	371 Hz
Dynamic Range [c]	200 Ω
I_{body} [c]	280 μA_{rms}
Resolution [c]	0.2 Ω
Mean Error in R [c]	0.4 Ω
Mean Error in X [c]	0.54 Ω
Accelerometer (3-axis)	
Bandwidth [d]	125 Hz, 62.5 Hz
Noise Density	150 µg/√Hz
Sample Rate [d, e]	250 Hz [255.8 Hz], 100 Hz [107.5 Hz]
Gyroscope (3-axis)	
Bandwidth	32 Hz
Noise	0.1°/s (rms, BW=47Hz, @0.014°/s/√Hz)
Sample Rate [d]	100 Hz [100 Hz]
Temperature Sensor	
Averaging	8 samples
Noise	7.8125°C (±1 LSB)
Sample Rate	1 Hz [0.996 Hz]
Data Storage Capacity	Card dependent

[a] Dependent on impedance load
[b] Dependent on SD card
[c] Reproduced from [33]
[d] Two values because one sensor is oversampled
[e] Programmed frequency [measured frequency]

demonstrating the ADC's sharp filter, as the roll-off of just the analog is only -47 dB/decade.

The main board has a minimum 33-hour battery life using a 500 mAh battery, though this is dependent on the impedance load. The average current consumption is ~14 mA, which is largely dominated by the gyroscopes' continuous current draw of 10 mA. Additionally, the largest current surges occur when turning on/off the EBI analog, reaching nearly 67 mA. During an EBI sweep lasting 2.68 s, the average current is ~34.7 mA.

The data outputs from the sensors were tested and validated using benchtop equipment to verify that the system yielded accurate measurements. For the audio board, the AFE was characterized using a signal analyzer (SR785, Dynamic Signal Analyzer, Stanford Research Systems, Sunnyvale, CA) and oscilloscope (DSOX3024A Oscilloscope, Keysight Technologies, Santa Rosa, CA). Additionally, the AFE and ADC outputs were compared to known input signals of various amplitudes, wave topologies, and frequencies. The EBI system architecture was extensively characterized in [33], and we validated that the data outputs from the brace matched the expected resistance and reactance values for known loads at every excitation frequency. For the IMUs, we validated the sensor outputs by comparing the acceleration and gyroscope values of the brace sensors when affixed to Xsens IMU units (MTW-38A70G20, Xsens, Enschede, The Netherlands). Lastly, we verified the temperature sensors' readings using a resistance temperature detector (RTD) (HH126, Omega Engineering, Stamford, CT).

B. Drop Sample Analysis

For the audio board, the drop sample analysis recording concluded once the battery died at nine hours. Since the audio board does not capture a timestamp for each individual audio sample but instead timestamps a group of audio samples, this analysis actually examines if a block of data, consisting of 2752 samples of 16-bit data from four channels, is dropped. Theoretically, given the size of the buffer and the sample rate, a data packet contains 58.7 ms of audio data. For the entire recording, the time between successive data blocks was calculated. The observed time differences between blocks were either 58.6 ms or 58.8 ms. This 0.2-ms artifact is a result of the timer resolution, which is ~0.2 ms. In short, for the nine-hour recording, no data blocks were dropped.

Unlike the audio board, data acquired with the main board were analyzed on a sample-by-sample basis, as a timestamp for each sample was captured. The recording analyzed was 35 hours long. Sampling for this board is driven by the data-ready interrupt of one the accelerometers, ACC0, which is programmed at 250 Hz. Samples for ACC0 clustered around an average sample period of approximately 3.91 ms, or 16 timer ticks. While there was a distribution of observed sample rates, they were within ±2 tick values around the 16-timer tick value, which is likely an artifact of the timer resolution and accelerometer internal timer accuracy. The other accelerometer (ACC1) and the gyroscopes (GYR0 and GYR1) are programmed to sample at 100 Hz. The sensors showed no dropped samples with average measured sample periods of 9.3, 10, and 10 ms for ACC1, GYR0, and GYR1, respectively. Similarly, the temperature sensors exhibited no dropped samples with an average period of 1.004 s, while the impedance sweeps were measured approximately every 46.17 s. Like the audio board, this board experienced no dropped samples.

Though we observed no dropped samples, in the instance that samples are dropped, timestamps of the data will allow for researchers to detect the length (time) of the missed data and determine the appropriate response. Depending on how

many samples are dropped, data can be reconstructed (e.g., a few dropped accelerometer samples may be interpolated) or removed entirely from analysis (e.g., prolonged periods of missing data).

C. Proof-of-Concept Recording Results

The signals from the proof-of-concept recordings are plotted in Fig. 5. For the joint sound measurement (Fig. 5(a)), joint sounds and IMU data were recorded from the audio and main boards, respectively. Given these boards are time-synchronized, joint sounds can be directly correlated with joint angle, as processed from the IMU data. Importantly, as shown in Fig. 5(a), significant acoustic emissions occur at similar joint angles for repeated exercises, which is consistent with our previous work that demonstrated—using benchtop equipment and electret microphones—that "clicks" (i.e., high-amplitude, short-duration, broad bandwidth signatures) occur at consistent joint angles for flexion/extension movements [13].

EBI measurements for 10 sweeps and the ensemble average of the sweeps are plotted in Fig. 5(b). Of note, individual sweeps are within 1 Ω of the ensemble average, showing repeatability for the static measurement. Further, the curve is consistent with the Fricke-Morse bioimpedance model, which represents tissue segments as a resistor in parallel with a series network of a resistor and capacitor, representing extra- and intra-cellular regions of tissue, respectively.

D. Limitations

1) Main Board Battery Life: The battery life of main board system can be improved. Currently, it is limited by the average current draw of the IMUs used in this design, specifically the gyroscope of the unit, which draws nearly 5 mA continuously (10 mA for the two used in this system) because this sensor cannot be put to sleep at the 100 Hz sample rate given its long wakeup time. This IMU was selected to allow for future iterations to readily integrate a magnetometer if necessary. If deemed unnecessary, power consumption may be lowered by exchanging this part for low-power, standalone accelerometers and gyroscopes or a combined package. If a magnetometer is required, a newer version of this part, which was recently released at the time of writing this paper, is available and draws less current, though other IMUs may be selected. Moreover, other power-saving techniques may be employed, such as intelligent, activity-based gating of sensor sampling, capturing only the relevant sensors' data and/or at their minimal sample rate.

2) Adhesive-Based Brace: The brace presented in this work leverages the use of adhesives: the microphone pads and EBI gel electrodes. These adhesives are not conducive for long-term wear, so dry alternatives should be considered for a deployable system. With respect to the contact microphones, such methods must achieve consistent and firm coupling with the skin to capture the joint acoustic signals, and these methods must not add significant noise to the signal during articulation of the knee. Moreover, the brace design itself must not degrade the signal quality with noise sourced from rubbing, brace slippage, or ill-fitting designs. For the electrodes, various metals (preferably those that do not corrode), conductive textiles, and other materials may be evaluated with a particular focus on accuracy, signal-to-noise ratio, and power requirements given the increase in the electrode-to-skin interface impedance [36]. Similar to the microphones, coupling mechanisms to ensure skin contact must be considered. Sanitation and other medical-grade factors when selecting such materials may present additional design constraints.

3) Prototype, Proof-of-Concept Form Factor: The design in this work primarily serves as a proof-of-concept for untethered measurements of joint health, though in its current form, it may be used for in-lab/in-clinic experiments. For example, this brace may immediately replace DAQ-based equipment currently used, especially for clinic-based studies where space is often extremely limited.

However, future designs must be optimized for at-home and long-term use. Importantly, efforts to improve upon the form factor—perhaps by adapting the current design to emulate or even retrofit a more traditional brace—could increase user compliance and acceptance of the device [37]. Further, retrofitting a hinged brace, for example, may allow for improved cable management and overall streamlining of the system (i.e., more closely fitted to the body), which would improve comfort and conformity between device and user. Additionally, weatherproofing should be considered to protect the system; for example, utilization of waterproof connectors and other packaging solutions would help prevent rain, sweat, debris, etc., from damaging the electronics.

V. Conclusion

This paper describes the design and validation of a smart, multimodal knee brace for joint health assessment. Custom electronics, firmware, and packaging were developed to provide a comprehensive sensor suite—encompassing joint acoustical emissions, EBI, inertial, and skin temperature data. These data are robustly sampled and saved to on-board storage without dropping packets. Tools, including the implementation of a host computer program and a stencil mechanism for determining sensor placement, were developed and implemented to allow users to interact with the device with minimal training while still achieving high-quality recordings. A 3D-printed brace served to easily place the sensors on the body and house all the electronics. Though this work was developed with the joint health application in mind, other areas may utilize a similar architecture to achieve wearable sensing, in particular with high-rate sensors.

In the immediate future, we anticipate this system being used in-clinic given its accessible form (vs. setting up cabled data acquisition units within an often small examination room). The easy-to-use system can be readily deployed by physicians and/or study coordinators with access to large clinical populations and their associated medical records. Such studies may enable greater understanding of joint sound signals, as knowledge of these signals and their properties is still in its infancy, largely due to a lack of cross-sectional databases and research exploring the origin and propagation of the signals.

Moreover, the joint sound data that has been collected has been limited to measurements recorded during simple motions,

namely seated flexion/extension, sit-to-stand (or squatting/leg-press) maneuvers, and, less frequently, treadmill walking. These exercises have been leveraged due to their simplicity, which, from a research perspective, aids the validity of controlled, repeated-measures experiments and also mitigates certain limitations imposed by cables, such as noise produced by cable motion and constraints on the distance a subject may travel from a wired DAQ. An untethered system can accommodate more complex motions and everyday activities, possibly enriching datasets for understanding physiological responses to different biomechanical conditions.

Likewise, the scope of these studies can be expanded beyond the clinic with a wearable system. At-home studies may be of interest for long-term monitoring of medication efficacy or rehabilitation progress, and telemedicine (or mHealth) is directly relevant to current needs in the joint health space. For example, pediatric rheumatology may benefit greatly from telemedicine; given a low supply of specialists, families are often required to travel far distances, incurring significant financial and time costs, especially when factoring the need for multiple visits [38]. A system which could readily classify a successful medication regimen, for example, may be particularly useful and potentially save patients an unnecessary trip to the clinic. Further, at-home studies may examine changes in joint health status throughout the course of a day. For example, patients with osteoarthritis report stiffness of the joint in the morning or after long periods of inactivity [39]. The brace may be used to record data immediately after a patient wakes in such cases or may even be used to explore whether the joint follows some circadian pattern like those followed by other physiological signals such as blood pressure [40]. These throughout-the-day measurements cannot be readily obtained with current clinical tools, and thus our design presents an opportunity to measure unique, rich, quantitative data. Ultimately, we envision this work will serve as the fundamental electronic design for future braces, thus deepening our understanding of sensorized joint health monitoring and broadening its applications.

REFERENCES

[1] L.-K. Shark, "Discovering differences in acoustic emission between healthy and osteoarthritic knees using a four-phase model of sit-stand-sit movements," *Open Med. Informat. J.*, vol. 4, no. 1, pp. 116–125, Aug. 2010.

[2] M. Sarillee, M. Hariharan, M. N. Anas, M. I. Omar, M. N. Aishah, and Q. W. Oung, "Assessment of knee joint abnormality using acoustic emission sensors," in *Proc. IEEE Int. Conf. Control Syst., Comput. Eng. (ICCSCE)*, Nov. 2014, pp. 378–383.

[3] J.-H. Lee, C.-C. Jiang, and T.-T. Yuan, "Vibration arthrometry in patients with knee joint disorders," *IEEE Trans. Biomed. Eng.*, vol. 47, no. 8, pp. 1131–1133, Aug. 2000.

[4] B. Semiz, S. Hersek, D. C. Whittingslow, L. A. Ponder, S. Prahalad, and O. T. Inan, "Using knee acoustical emissions for sensing joint health in patients with juvenile idiopathic arthritis: A pilot study," *IEEE Sensors J.*, vol. 18, no. 22, pp. 9128–9136, Nov. 2018.

[5] S. Hersek *et al.*, "Acoustical emission analysis by unsupervised graph mining: A novel biomarker of knee health status," *IEEE Trans. Biomed. Eng.*, vol. 65, no. 6, pp. 1291–1300, Jun. 2018.

[6] H.-K. Jeong, M. B. Pouyan, D. C. Whittingslow, V. Ganti, and O. T. Inan, "Quantifying the effects of increasing mechanical stress on knee acoustical emissions using unsupervised graph mining," *IEEE Trans. Neural Syst. Rehabil. Eng.*, vol. 26, no. 3, pp. 594–601, Mar. 2018.

[7] U. G. Kyle *et al.*, "Bioelectrical impedance analysis—Part I: Review of principles and methods," *Clin. Nutrition*, vol. 23, no. 5, pp. 1226–1243, Oct. 2004.

[8] S. Hersek *et al.*, "Wearable vector electrical bioimpedance system to assess knee joint health," *IEEE Trans. Biomed. Eng.*, vol. 64, no. 10, pp. 2353–2360, Oct. 2017.

[9] R. Kianifar, A. Lee, S. Raina, and D. Kulic, "Automated assessment of dynamic knee valgus and risk of knee injury during the single leg squat," *IEEE J. Transl. Eng. Health Med.*, vol. 5, Oct. 2017, Art. no. 2100213.

[10] T. Seel, J. Raisch, and T. Schauer, "IMU-based joint angle measurement for gait analysis," *Sensors*, vol. 14, no. 4, pp. 6891–6909, 2014.

[11] R. A. Bloomfield, M. C. Fennema, K. A. McIsaac, and M. G. Teeter, "Proposal and validation of a knee measurement system for patients with osteoarthritis," *IEEE Trans. Biomed. Eng.*, vol. 66, no. 2, pp. 319–326, Feb. 2019.

[12] H. Dejnabadi, B. M. Jolles, E. Casanova, P. Fua, and K. Aminian, "Estimation and visualization of sagittal kinematics of lower limbs orientation using body-fixed sensors," *IEEE Trans. Biomed. Eng.*, vol. 53, no. 7, pp. 1385–1393, Jul. 2006.

[13] C. N. Teague *et al.*, "Novel methods for sensing acoustical emissions from the knee for wearable joint health assessment," *IEEE Trans. Biomed. Eng.*, vol. 63, no. 8, pp. 1581–1590, Aug. 2016.

[14] Q. Liu *et al.*, "Gazelle: Energy-efficient wearable analysis for running," *IEEE Trans. Mobile Comput.*, vol. 16, no. 9, pp. 2531–2544, Sep. 2017.

[15] S. Hersek, H. Toreyin, and O. T. Inan, "A robust system for longitudinal knee joint edema and blood flow assessment based on vector bioimpedance measurements," *IEEE Trans. Biomed. Circuits Syst.*, vol. 10, no. 3, pp. 545–555, Jun. 2016.

[16] A. Hafid, S. Benouar, M. Kedir-Talha, F. Abtahi, M. Attari, and F. Seoane, "Full impedance cardiography measurement device using raspberry PI3 and system-on-chip biomedical instrumentation solutions," *IEEE J. Biomed. Health Informat.*, vol. 22, no. 6, pp. 1883–1894, Nov. 2018.

[17] T. Vuorela, V.-P. Seppa, J. Vanhala, and J. Hyttinen, "Design and implementation of a portable long-term physiological signal recorder," *IEEE Trans. Inf. Technol. Biomed.*, vol. 14, no. 3, pp. 718–725, May 2010.

[18] M. Rapin *et al.*, "Wearable sensors for frequency-multiplexed EIT and multilead ECG data acquisition," *IEEE Trans. Biomed. Eng.*, vol. 66, no. 3, pp. 810–820, Mar. 2019.

[19] Y. Athavale and S. Krishnan, "A telehealth system framework for assessing knee-joint conditions using vibroarthrographic signals," *Biomed. Signal Process. Control*, vol. 55, Jan. 2020, Art. no. 101580.

[20] K. C. Barr and K. Asanović, "Energy-aware lossless data compression," *ACM Trans. Comput. Syst.*, vol. 24, no. 3, pp. 250–291, Aug. 2006.

[21] A. Martin and J. Voix, "In-ear audio wearable: Measurement of heart and breathing rates for health and safety monitoring," *IEEE Trans. Biomed. Eng.*, vol. 65, no. 6, pp. 1256–1263, Jun. 2018.

[22] D. D. Mehta, M. Zañartu, S. W. Feng, H. A. Cheyne, and R. E. Hillman, "Mobile voice health monitoring using a wearable accelerometer sensor and a smartphone platform," *IEEE Trans. Biomed. Eng.*, vol. 59, no. 11, pp. 3090–3096, Nov. 2012.

[23] B. Travaglione *et al.*, "Using low cost single-board microcontrollers to record underwater acoustical data," in *Proc. Internoise Conf.*, Melbourne, NSW, Australia, Nov. 2014, pp. 1–8.

[24] B. Travaglione, "Using a single-board microcontroller and ADC to perform real-time sonar signal processing," in *Proc. Acoust., 2nd Austral. Acoust. Soc. Conf.*, Melbourne, NSW, Australia, Nov. 2016, pp. 1–8.

[25] C.-C. Wang, Y.-H. Hsiao, and M.-C. Huang, "Development of MSP430-based ultra-low power expandable underwater acoustic recorder," *Ocean Eng.*, vol. 36, nos. 6–7, pp. 446–455, May 2009.

[26] M. Caldas-Morgan, A. Alvarez-Rosario, and L. Rodrigues Padovese, "An autonomous underwater recorder based on a single board computer," *PLoS ONE*, vol. 10, no. 6, 2015, Art. no. e0130297.

[27] B. Gao and W. L. Woo, "Wearable audio monitoring: Content-based processing methodology and implementation," *IEEE Trans. Human-Mach. Syst.*, vol. 44, no. 2, pp. 222–233, Apr. 2014.

[28] A. P. Hill, P. Prince, E. Piña Covarrubias, C. P. Doncaster, J. L. Snaddon, and A. Rogers, "AudioMoth: Evaluation of a smart open acoustic device for monitoring biodiversity and the environment," *Methods Ecology Evol.*, vol. 9, no. 5, pp. 1199–1211, May 2018.

[29] O. T. Inan *et al.*, "Wearable knee health system employing novel physiological biomarkers," *J. Appl. Physiol.*, vol. 124, no. 3, pp. 537–547, Mar. 2018.

[30] *SD Specifications: Part 1 Physical Layer Simplified Specification*, SD Association, San Ramon, CA, USA, 2016.

[31] M. Etemadi, O. T. Inan, J. A. Heller, S. Hersek, L. Klein, and S. Roy, "A wearable patch to enable long-term monitoring of environmental, activity and hemodynamics variables," *IEEE Trans. Biomed. Circuits Syst.*, vol. 10, no. 2, pp. 280–288, Apr. 2016.
[32] S. O. H. Madgwick, A. J. L. Harrison, and R. Vaidyanathan, "Estimation of IMU and MARG orientation using a gradient descent algorithm," in *Proc. IEEE Int. Conf. Rehabil. Robot.*, Jun. 2011, pp. 1–7.
[33] S. Mabrouk *et al.*, "Robust longitudinal ankle edema assessment using wearable bioimpedance spectroscopy," *IEEE Trans. Biomed. Eng.*, vol. 67, no. 4, pp. 1019–1029, Apr. 2020.
[34] *Medical Electrical Equipment-Part 1-11: General Requirements for Basic Safety and Essential Performance-Collateral Standard: Requirements for Medical Electrical Equipment and Medical Electrical Systems Used in the Home Healthcare Environment*, IEC document 60601-1-11, 2015.
[35] T. McGrath, R. Fineman, and L. Stirling, "An auto-calibrating knee flexion-extension axis estimator using principal component analysis with inertial sensors," *Sensors*, vol. 18, no. 6, p. 1882, Jun. 2018.
[36] Y. M. Chi, T.-P. Jung, and G. Cauwenberghs, "Dry-contact and noncontact biopotential electrodes: Methodological review," *IEEE Rev. Biomed. Eng.*, vol. 3, pp. 106–119, 2010.
[37] J. R. Basford and S. J. Johnson, "Form may be as important as function in orthotic acceptance: A case report," *Arch. Phys. Med. Rehabil.*, vol. 83, no. 3, pp. 433–435, Mar. 2002.
[38] E. A. Kessler, A. K. Sherman, and M. L. Becker, "Decreasing patient cost and travel time through pediatric rheumatology telemedicine visits," *Pediatric Rheumatol.*, vol. 14, no. 1, p. 54, Dec. 2016.
[39] R. D. Altman *et al.*, "Recommendations for the medical management of osteoarthritis of the hip and knee: 2000 Update," *Arthritis Rheumatism*, vol. 43, no. 9, pp. 1905–1915, Sep. 2000.
[40] M. W. Millar-Craig, C. N. Bishop, and E. B. Raftery, "Circadian variation of blood-pressure," *Lancet*, vol. 311, no. 8068, pp. 795–797, Apr. 1978.

Caitlin N. Teague (Student Member, IEEE) received the B.S. degree in electrical engineering and the M.S. and Ph.D. degrees in electrical and computer engineering from the Georgia Institute of Technology (Georgia Tech), Atlanta, GA, USA, in 2014, 2016, and 2020, respectively.

She is a Recent Doctoral Graduate, completing her research as a member of Dr. Omer T. Inan's lab. She will begin a postdoctoral position in a similar health-focused field shortly. Her research interests include development of noninvasive biomedical devices and systems, particularly those that enable at-home, long-term physiological monitoring. She received the President's Fellowship from Georgia Tech in 2014.

J. Alex Heller (Member, IEEE) received the B.S. degree in mechanical engineering from the University of Southern California, Los Angeles, CA, USA, in 2008, and the M.S. degree in bioengineering from the University of California, San Francisco (UCSF)/UC Berkeley Joint Graduate Group in 2013.

In 2008, he joined Northrop Grumman, Marine Systems, Sunnyvale, CA, USA, as a Mechanical Engineer. In 2010, he joined Biodesign Laboratory and the Pediatric Device Consortium at UCSF as an Engineer and a Researcher, where he worked on renal replacement therapy, home monitoring of chronic disease, and obstetrics related medical devices. Since 2016, he has been an Engineer with the Etemadi Research Group and Northwestern University, Chicago, IL, USA.

Brandi N. Nevius was born in Matthews, NC, USA, in 1993. She received the B.S. degree in biomedical engineering from the Georgia Institute of Technology, Atlanta, GA, USA, in 2016, where she is currently pursuing the M.S. degree in mechanical engineering.

From 2016 to 2018, she was the Lead Biomedical Engineer and the Project Manager with Motus Nova, a small biomedical company centered on the design, manufacture, and deployment of two tele-robotic stroke rehabilitation devices. She is also a Graduate Research Assistant with the Inan Research Lab, Georgia Tech, focusing on developing and accessing novel biomedical wearables.

Andrew M. Carek received the B.S. degree in electrical engineering from Clemson University, Clemson, SC, USA, in 2014, and the M.S. and Ph.D. degrees in electrical engineering from the Georgia Institute of Technology, Atlanta, GA, USA, in 2016 and 2019, respectively.

He is currently a Postdoctoral Researcher with the Department of Anesthesiology, Northwestern University, Chicago, IL, USA. His research interests include development of noninvasive physiological monitoring systems for human health assessment both in the clinic and at home.

Samer Mabrouk was born in Cairo, Egypt, in 1992. He received the B.S. degree in electrical and computer engineering from the Georgia Institute of Technology, Atlanta, GA, USA, in 2015 after transferring from the American University, Cairo, in 2013, and the M.S degree in electrical and computer engineering from the Georgia Institute of Technology, in 2019.

Throughout his undergrad, he interned at Schlumberger, Panasonic and Tesla as an Embedded Systems Intern. At Panasonic, he worked in the Advanced Engineering Department on researching and designing cutting edge technologies for future infotainment system that will be presented in CES. After his undergrad, he joined Dell as a full-time Software Development Engineer, working on designing and developing a test automation system to be used in overseas OEMs. In 2017, he joined Inan Research Lab as a Graduate Research Assistant. His research focuses on miniaturizing wearable sensors that use bioimpedance and algorithms that allow robust tracking of a tissue's static fluid for the applications of joint edema tracking and IV infiltration detection.

Florencia Garcia-Vicente received the B.A. degree in mathematical economics from the Pomona College, Claremont, CA, USA, in 2013. She is currently pursuing the M.S. degree in computer science with Northwestern University, Evanston, IL, USA.

In September of 2013, she joined FTI Consulting as a Consultant working on restructuring cases. In May 2015, she joined a startup called Belly as a Platform Engineer. In November 2016, she joined the Etemadi Research Group as an Engineer in Chicago, IL, USA.

Omer T. Inan (Senior Member, IEEE) received the B.S., M.S., and Ph.D. degrees in electrical engineering from Stanford University, Stanford, CA, USA, in 2004, 2005, and 2009, respectively.

He joined ALZA Corporation (A Johnson and Johnson Company) in 2006, where he designed micropower circuits for iontophoretic drug delivery. In 2007, he joined Countryman Associates, Inc., Menlo Park, CA, USA, where he was the Chief Engineer, involved in designing and developing high-end professional audio circuits and systems. From 2009 to 2013, he was also a Visiting Scholar with the Department of Electrical Engineering, Stanford University. From 2013 to 2018, he was an Assistant Professor of Electrical and Computer Engineering with the Georgia Institute of Technology, where he is currently an Associate Professor. He is also an Adjunct Associate Professor with the Wallace H. Coulter Department of Biomedical Engineering. He has published more than 180 technical articles in peer-reviewed international journals and conferences, and has six issued patents. His research focuses on non-invasive physiologic sensing and modulation for human health and performance, including for chronic disease management, acute musculoskeletal injuries and disorders, and pediatric care.

Dr. Inan received the Gerald J. Lieberman Fellowship in 2009, the Lockheed Dean's Excellence in Teaching Award in 2016, the Sigma Xi Young Faculty Award in 2017, the IEEE Sensors Early Career Award in 2018, the Office of Naval Research Young Investigator Award in 2018, and the National Science Foundation CAREER Award in 2018. He was a National Collegiate Athletic Association (NCAA) All-American in the discus throw for three consecutive years from 2001 to 2003. He is an Associate Editor of the IEEE JOURNAL OF BIOMEDICAL AND HEALTH INFORMATICS, a Theme 10 Co-Editor of the IEEE Engineering in Medicine and Biology Conference, an Associate Editor of the IEEE Biomedical and Health Informatics Conference, an Invited Member of the IEEE Technical Committee on Translational Engineering for Healthcare Innovation and the IEEE Technical Committee on Cardiopulmonary Systems, and a Technical Program Committee Member or the Track Chair for several other major international biomedical engineering conferences.

Mozziyar Etemadi (Member, IEEE) received the B.S. and M.S. degrees in electrical engineering from Stanford University, Stanford, CA, USA, in 2008 and June 2009, respectively, and the Ph.D. degree in bioengineering from the University of California at San Francisco (UCSF), CA, USA/University of California at Berkeley, CA, USA, Joint Graduate Group in Bioengineering, in 2013, and the M.D. degree in 2016, from UCSF in 2016 as part of the Medical Scientist Training Program.

He is currently a Research Assistant Professor with the Department of Anesthesiology and the Department of Biomedical Engineering, Northwestern University, Chicago, IL, USA.

Dr. Etemadi was named Forbes magazine's 30 Under 30 in Science in January 2012. Later that year, he received the Center for Integration of Medicine and Innovative Technology (CIMIT) Prize for Primary Care Innovation, and the grand prize in the Dow Sustainability Student Innovation Challenge. In 2011, he helped lead a Research Team in the Vodafone Americas Wireless Innovation Challenge and the mHealth Alliance Award to second prize. In 2009, while at Stanford University, he received the Frederick E. Terman Award for Scholastic Achievement in Engineering and also received the Electrical Engineering Fellowship, providing full support for his graduate studies.